Lawrence Berkeley National Laboratory

Title
Robustness of magnetic and electric domains against charge carrier doping in multiferroic hexagonal ErMnO3

Permalink
https://escholarship.org/uc/item/27t4862d

Authors
Hassanpour, E
Wegmayr, V
Schaab, J
et al.

You may also be interested in:

Functional domain walls in multiferroics
Dennis Meier

Robust templates for domain boundary engineering in ErMnO3
Ekhard K H Salje

Characteristics and controllability of vortices in ferromagnetics, ferroelectrics, and
multiferroics
Yue Zheng and W J Chen

Pressure and strain effects of hexagonal rare-earth manganites: a first-principles study
Hengxin Tan, Changsong Xu, Menglei Li et al.

New modalities of strain-control of ferroelectric thin films
Anoop R Damodaran, Joshua C Agar, Shishir Pandya et al.

Multiferroics and magnetoelectrics: thin films and nanostructures
L W Martin, S P Crane, Y-H Chu et al.

Common features of low-temperature spin–charge separation and superlattice formation in
multiferroic manganites and antiferromagnetic cuprates
V A Sanina, E I Golovenchits, V G Zalesskii et al.

The 2016 oxide electronic materials and oxide interfaces roadmap
M Lorenz, M S Ramachandra Rao, T Venkatesan et al.

New Journal of Physics

The open access journal at the forefront of physics

PAPER

Robustness of magnetic and electric domains against charge carrier doping in multiferroic hexagonal ErMnO₃

E Hassanpour[1], V Wegmayr[1], J Schaab[1], Z Yan[2], E Bourret[2], Th Lottermoser[1], M Fiebig[1] and D Meier[1]

1 Department of Materials, ETH Zürich, 8093 Zürich, Switzerland
2 Materials Science Division, Lawrence Berkeley National Laboratory, Berkeley, CA 94720, USA
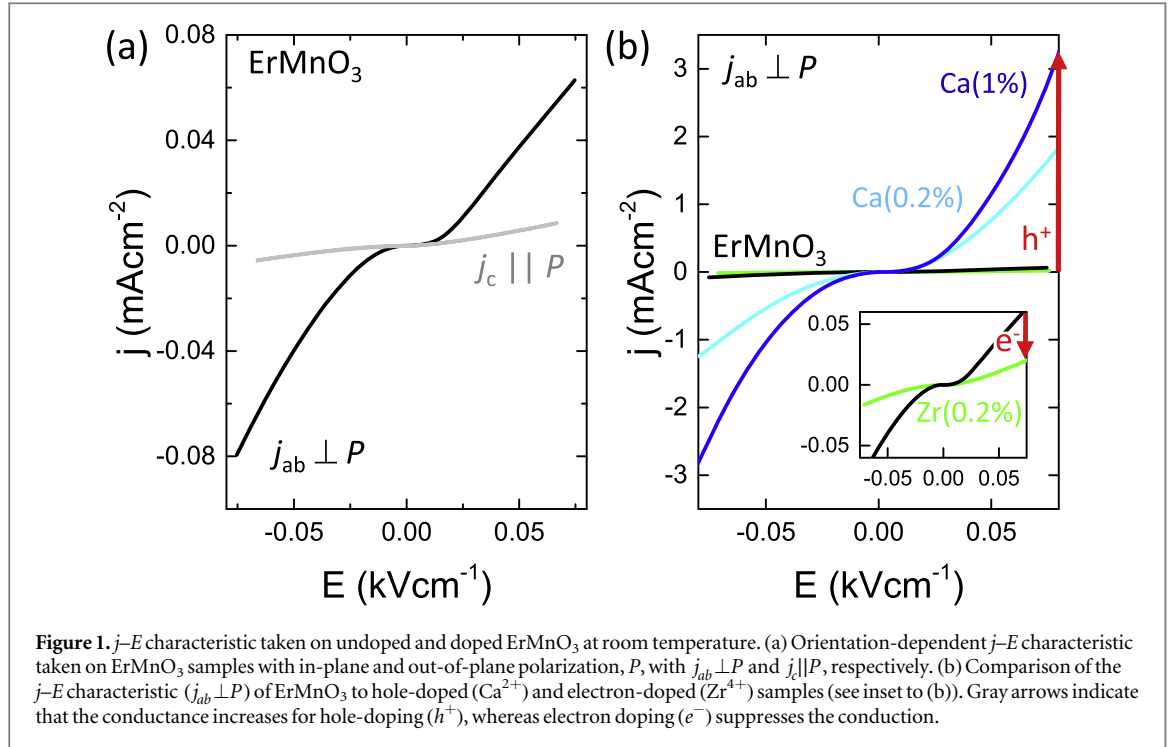
E-mail: dennis.meier@mat.ethz.ch

Abstract

We investigate the effect of chemical doping on the electric and magnetic domain pattern in multiferroic hexagonal ErMnO₃. Hole- and electron doping are achieved through the growth of $Er_{1-x}Ca_xMnO_3$ and $Er_{1-x}Zr_xMnO_3$ single crystals, which allows for a controlled introduction of divalent and tetravalent ions, respectively. Using conductance measurements, piezoresponse force microscopy and nonlinear optics we study doping-related variations in the electronic transport and image the corresponding ferroelectric and antiferromagnetic domains. We find that moderate doping levels allow for adjusting the electronic conduction properties of ErMnO₃ without destroying its characteristic domain patterns. Our findings demonstrate the feasibility of chemical doping for non-perturbative property-engineering of intrinsic domain states in this important class of multiferroics.

1. Introduction

The unique magnetoelectric properties of multiferroics are mainly determined by the coexistence and interaction of magnetic and electric domains [1, 2]. Over the last years, such magnetoelectric coupling phenomena were scrutinized in-depth and significant progress has been made in explaining the domain formation in archetypal multiferroics such as $TbMnO_3$, $MnWO_4$, and the hexagonal manganites $RMnO_3$ with $R = $ Sc, Y, In, Dy–Lu [3–5]. In the latter case it was shown that geometrically driven ferroelectric vortex domain structures emerge at $\gtrsim 1000$ K and that the size of these domains can readily be tuned by thermal annealing [6–9]. These ferroelectric domains are attracting great attention and serve, e.g., for explaining the formation of topological defects [8] or as source of intriguing interface effects [10]. At $T_N \approx 100$ K additional antiferromagnetic domains form and give rise to pronounced magnetoelectric domain and domain-wall couplings [5, 11, 12]. These magnetoelectric couplings are of great interest for the emergent field of domain engineering [13]. Analogous to the ferroelectric domains, the size of the magnetic domains can be adjusted through thermal annealing [14]. Despite these promising functional properties, however, most open challenges still relate to fundamental research. One of the key questions is how to tune the material properties towards a technologically feasible working range, without affecting the electric and magnetic order that give rise to the functional behavior.

A powerful procedure for modifying electronic material properties is the introduction of impurities. This is strikingly reflected by extrinsic semiconductors that owe their specific n- or p-type properties to implanted defects [15]. Following the same idea, different ionic impurities have been introduced to $RMnO_3$ systems with the goal to improve their magnetic response [16, 17] or electronic conductance [18]. It remains unclear, however, to what extent chemical doping affects the topology and functionality of the ferroelectric and antiferromagnetic domains as spatially resolved studies are virtually non-existent.

Here, we present such a study by investigating ferroelectric and magnetic domains in moderately doped hexagonal manganites. We show that the electronic conductance of ErMnO₃ can be tuned within a range of about two orders of magnitude by introducing either divalent (Ca^{2+}) or tetravalent (Zr^{4+}) ions into the system. Using piezoresponse force microscopy (PFM) and optical second harmonic generation (SHG) [19] we image the

Figure 1. *j–E* characteristic taken on undoped and doped $ErMnO_3$ at room temperature. (a) Orientation-dependent *j–E* characteristic taken on $ErMnO_3$ samples with in-plane and out-of-plane polarization, *P*, with $j_{ab} \perp P$ and $j_c \| P$, respectively. (b) Comparison of the *j–E* characteristic ($j_{ab} \perp P$) of $ErMnO_3$ to hole-doped (Ca^{2+}) and electron-doped (Zr^{4+}) samples (see inset to (b)). Gray arrows indicate that the conductance increases for hole-doping (h^+), whereas electron doping (e^-) suppresses the conduction.

ferroelectric and antiferromagnetic domain structures of doped and undoped $ErMnO_3$. We find that the key parameters of the multiferroic domain state, such as the formation of ferroelectric vortices and the pattern of antiferromagnetic domains, are robust against the applied ionic alteration, demonstrating the usability of chemical doping for enhancing the functionality of the geometric multiferroic domain state.

The parent compound of our doping series, $ErMnO_3$, exhibits geometrically driven improper ferroelectricity below $T_C = 1470$ K with the spontaneous polarization *P* oriented parallel to the hexagonal *c*-axis ($P\|c$) [7, 9]. The ferroelectric domain structure displays a characteristic vortex pattern composed of six ferroelectric domain states [6, 20]. Antiferromagnetic order, and with it multiferroicity, emerges at $T_N = 80$ K. A detailed discussion of the magnetic order of the Mn 3d- and Er 4f-moments can be found elsewhere [21, 22]. Regarding its electronic properties, $ErMnO_3$ is described as a small-band-gap p-type semiconductor ($E_{gap} = 1.8$ eV) [23].

2. Results

2.1. Samples
In order to tune the resistivity and study implications for the domain pattern, we adjusted the number of majority carriers (holes) by doping the system with divalent or tetravalent ions [18]. This was achieved by growing single crystals of $Er_{1-x}Ca_xMnO_3$ and $Er_{1-x}Zr_xMnO_3$ ($x \leqslant 0.01$) by the pressurized floating-zone technique [24]. For our experiments oriented platelets with lateral dimensions of about 5×5 mm^2 were cut and chemo-mechanically polished. The polishing yielded surfaces with a root mean square roughness of ≈ 0.5 nm.

2.2. Electronic transport
We begin our discussion by a comparison of the electronic transport properties of undoped, hole-doped, and electron-doped $ErMnO_3$ samples. Since we are only interested in relative values regarding the electronic transport, we measured the current–voltage (*j–E*) characteristic in a two-probe setup using Ag contacts. The results obtained at room temperature are summarized in figure 1. In figure 1(a) we present *j–E* measurements taken on disc-shaped $ErMnO_3$ samples with out-of-plane and in-plane polarization, so that $j_c\|P$ and $j_{ab}\perp P$, respectively. The nonlinear *j–E* data reflect a pronounced resistivity anisotropy and current values *j* that are comparable with data gained on $YMnO_3$, $LuMnO_3$, and $ScMnO_3$ [25, 26]. The difference between measurements with $j_c\|P$ and $j_{ab}\perp P$ originates from the layered Mn^{3+} arrangement in the hexagonal $RMnO_3$ systems and the two-dimensional character of their electronic structure [25]. In figure 1(b) we compare the $ErMnO_3$ data ($j_{ab}\perp P$) with *j–E* curves collected on $Er_{1-x}Ca_xMnO_3$ ($x = 0.002, 0.010$) and $Er_{1-x}Zr_xMnO_3$ ($x = 0.002$). The plot in figure 1(b) reveals a pronounced doping dependence of j_{ab}, showing significantly increased conductivity in the case of Ca^{2+}-doping and suppressed conductivity for Zr^{4+}-doping. Comparing the
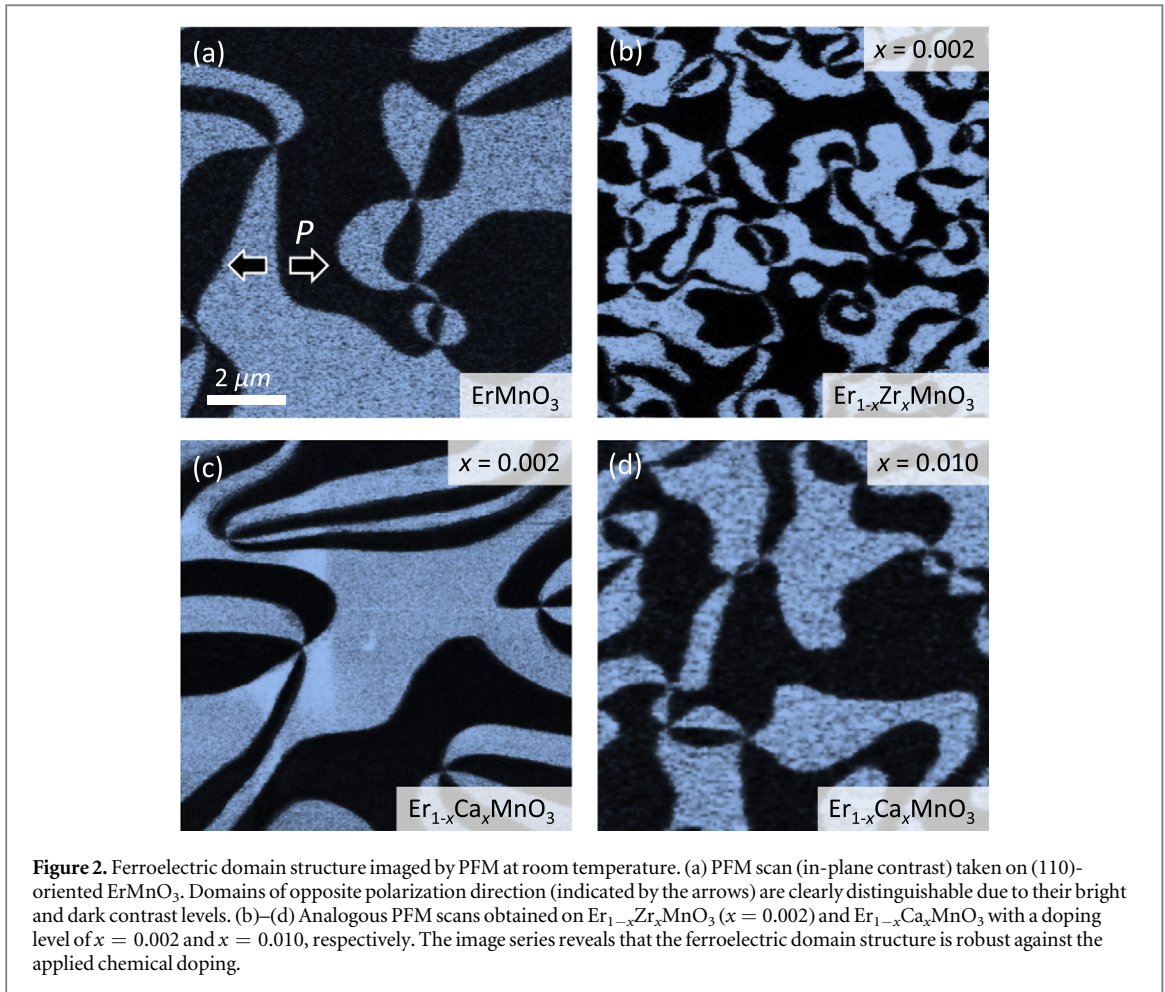
Figure 2. Ferroelectric domain structure imaged by PFM at room temperature. (a) PFM scan (in-plane contrast) taken on (110)-oriented ErMnO$_3$. Domains of opposite polarization direction (indicated by the arrows) are clearly distinguishable due to their bright and dark contrast levels. (b)–(d) Analogous PFM scans obtained on Er$_{1-x}$Zr$_x$MnO$_3$ ($x = 0.002$) and Er$_{1-x}$Ca$_x$MnO$_3$ with a doping level of $x = 0.002$ and $x = 0.010$, respectively. The image series reveals that the ferroelectric domain structure is robust against the applied chemical doping.
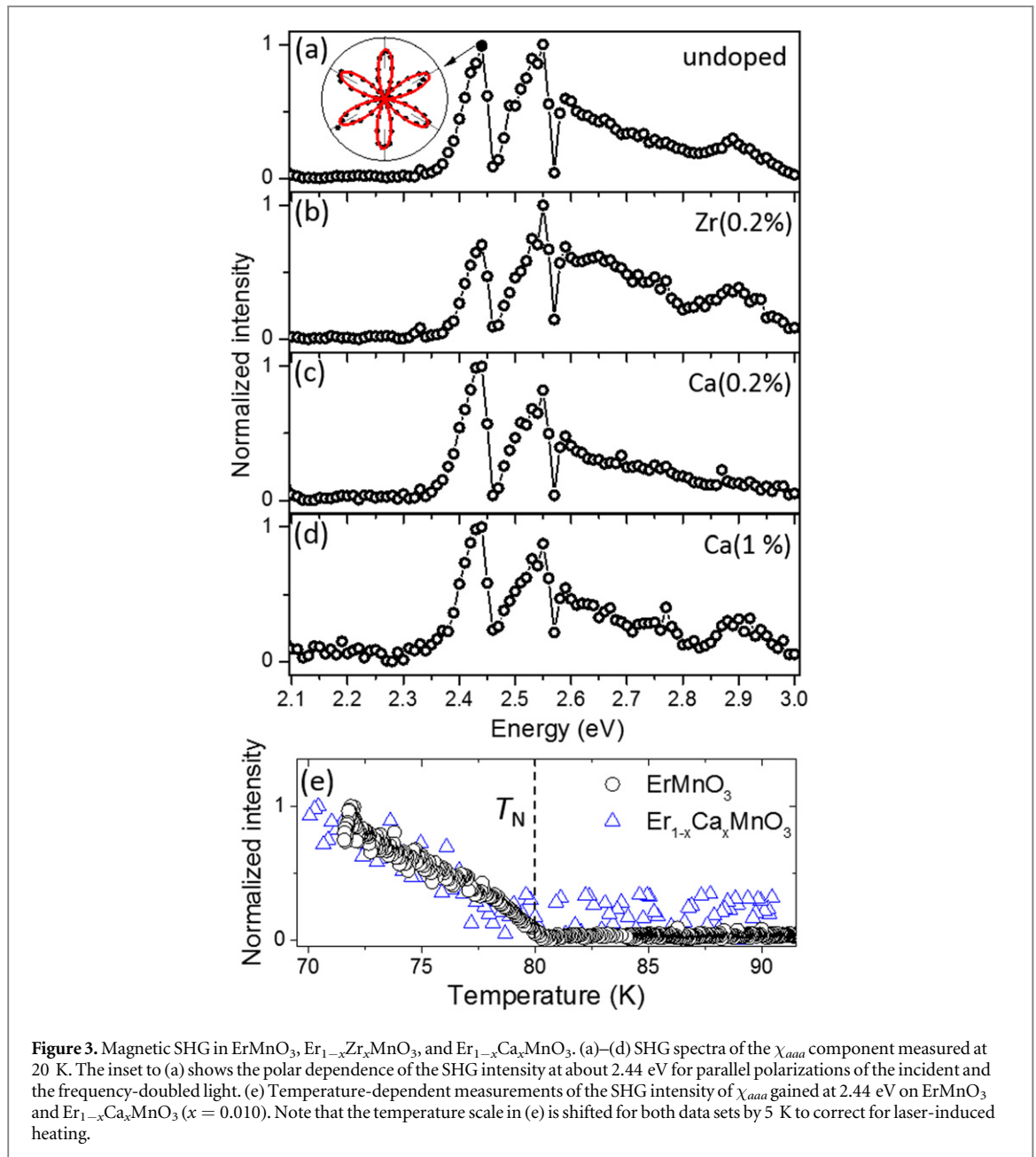
results for the maximum electric field we applied ($E = 0.075$ kV cm^{-1}), we find that j_{ab} varies by almost two orders of magnitude. We note that the observed trend, as well as the exponential decrease in j_{ab} towards low temperature (not shown), is consistent with the abovementioned p-type nature of ErMnO$_3$ [23]. Following Van Aken *et al* [18], the observed asymmetry in hole- and electron-doping can be explained based on band population: hole doping leads to occupation of the dispersive manganese xy and x^2-y^2 d-bands which results in a conductive state. In contrast, electron doping retains the insulating state as additional electrons will either compensate for holes or fill localized $3z^2-r^2$ bands with poor orbital overlap. Figure 1 thus demonstrates that the bulk conductivity was successfully varied by almost two orders of magnitude by the chemical doping.

2.3. Piezoresponse force microscopy
In the next step, we performed PFM scans on our samples to test the impact of chemical doping on the vortex nature of the ferroelectric domain structure. Since the ferroelectricity in ErMnO$_3$ is driven by space-filling effects and geometric constraints, the implementation of ionic lattice defects may alter or even suppress the characteristic vortex formation. PFM images obtained on undoped and doped samples with in-plane polarization are shown in figures 2(a)–(d). The scans were taken with an AC voltage of 5 V at ambient conditions and show the PFM in-plane contrast. Independent of the doping, the domain structures reflect the characteristic six-fold meeting points of alternating $+P$ (bright) and $-P$ (dark) domains [6, 20]. We note that the as-grown domains have an average size of a few micrometers, with the exception of Er$_{1-x}$Zr$_x$MnO$_3$, where the domains are slightly smaller, which can be attributed to faster cooling after synthesis [8, 9]. We deliberately preserved the as-grown state in order to avoid subsequent changes in stochiometry [27]. Based on the data presented in figures 1 and 2, we conclude that moderate chemical doping ($x \leqslant 0.01$) allows for tuning the bulk conductance within a range of about two orders of magnitude and that the vortex structure of the ferroelectric domains is robust against the applied implantation of ionic lattice defects.

2.4. Optical SHG
As discussed, the magnetic order in ErMnO$_3$ emerges independently of the electric one and at a significantly lower temperature. The spin structure is strongly frustrated so that subtle changes in the electronic stucture,

Figure 3. Magnetic SHG in ErMnO$_3$, Er$_{1-x}$Zr$_x$MnO$_3$, and Er$_{1-x}$Ca$_x$MnO$_3$. (a)–(d) SHG spectra of the χ_{aaa} component measured at 20 K. The inset to (a) shows the polar dependence of the SHG intensity at about 2.44 eV for parallel polarizations of the incident and the frequency-doubled light. (e) Temperature-dependent measurements of the SHG intensity of χ_{aaa} gained at 2.44 eV on ErMnO$_3$ and Er$_{1-x}$Ca$_x$MnO$_3$ ($x = 0.010$). Note that the temperature scale in (e) is shifted for both data sets by 5 K to correct for laser-induced heating.

such as the mixed Mn^{3+}-Mn^{2+} system created by the Zr^{4+} substitution [18], may lead to pronounced changes in the antiferromagnetic order and domains. In consequence, a higher sensitivity of the magnetic compared to the electric subsystem may be expected.

To analyze a possible dependence of the symmetry of the magnetic order and the associated domain pattern on chemical doping, we investigated our samples by optical SHG [19]. The corresponding process of optical frequency doubling is described by the equation [19]

$$P_i(2\omega) = \epsilon_0 \chi_{ijk} E_j(\omega) E_k(\omega). \tag{1}$$

A light field $\vec{E}$ at frequency ω is incident onto the sample, inducing a dipole oscillation $\vec{P}(2\omega)$, which acts as source of a frequency-doubled light wave. The susceptibility χ_{ijk} couples incident light fields with polarizations j and k to an SHG contribution with polarization i. Following the Neumann principle, symmetry determines the set of tensor components $\chi_{ijk} \neq 0$. The antiferromagnetic order of the Mn^{3+} spin system in RMnO$_3$ affects this symmetry, leading to characteristic contributions that allow for uniquely identifying the magnetic structure.

In figure 3 we present spatially integrated SHG spectroscopy data taken on c-oriented samples (P out of plane) with a thickness of about 80 μm in transmission geometry as described elsewhere [19]. Figure 3(a) shows the SHG spectrum of ErMnO$_3$ associated to the χ_{aaa} component ($T = 20$ K) [22]. The frequency-doubled signal was measured with light incident along the c direction and shows the characteristic six-fold polar dependence,
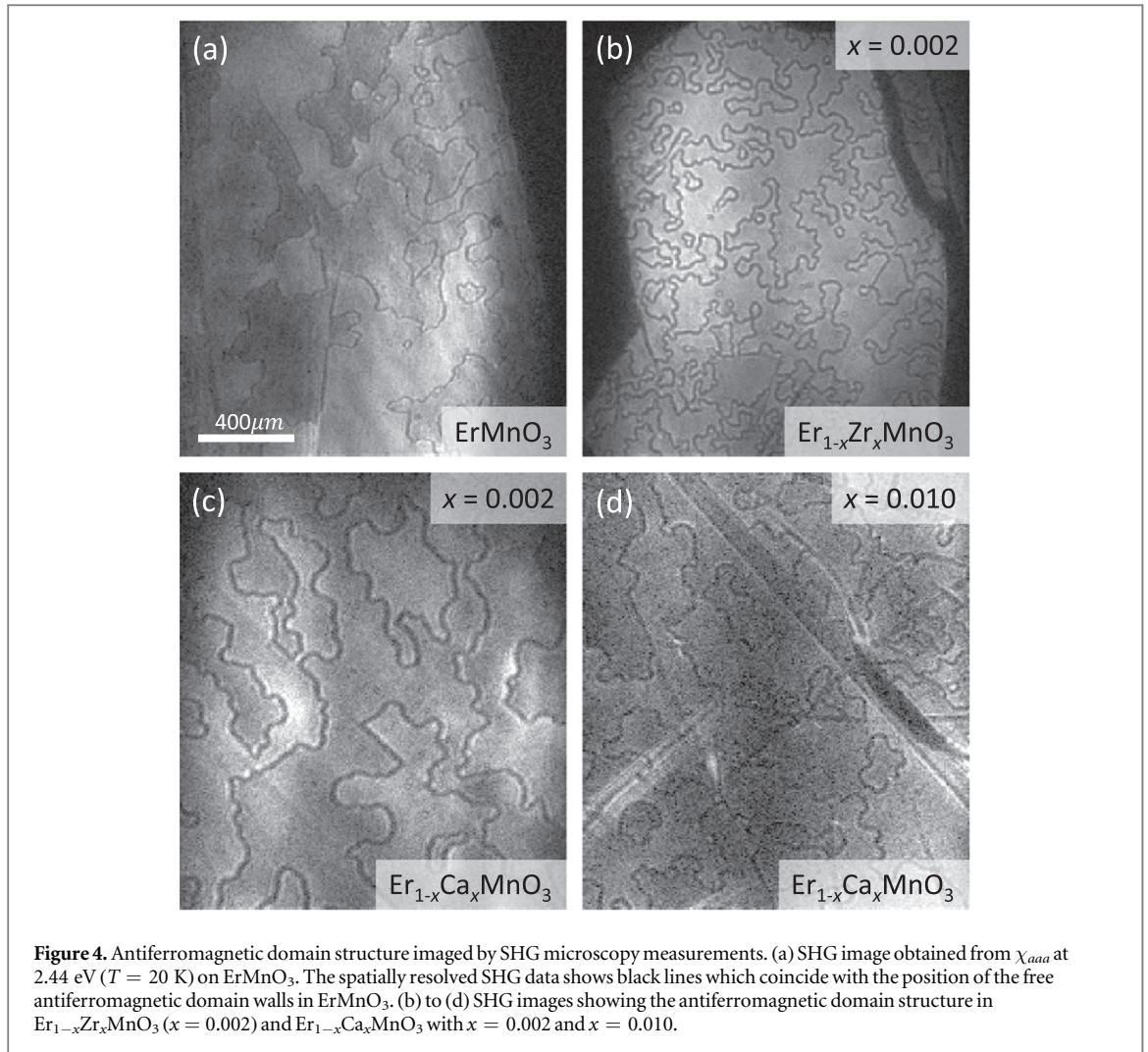
Figure 4. Antiferromagnetic domain structure imaged by SHG microscopy measurements. (a) SHG image obtained from χ_{aaa} at 2.44 eV ($T = 20$ K) on ErMnO$_3$. The spatially resolved SHG data shows black lines which coincide with the position of the free antiferromagnetic domain walls in ErMnO$_3$. (b) to (d) SHG images showing the antiferromagnetic domain structure in Er$_{1-x}$Zr$_x$MnO$_3$ ($x = 0.002$) and Er$_{1-x}$Ca$_x$MnO$_3$ with $x = 0.002$ and $x = 0.010$.

which reflects the coupling to the triangular antiferromagnetic ordering of the Mn^{3+} spins according to the so-called Γ_4-symmetry (see inset to figure 3(a)) [22, 28]. The fine structure of the ErMnO$_3$ spectrum has been explained by Iizuka-Sakano *et al* based on the exchange of neighboring Mn^{3+} ions [29]. Magnetic SHG spectra taken under the same conditions on Er$_{1-x}$Zr$_x$MnO$_3$ and Er$_{1-x}$Ca$_x$MnO$_3$ are presented in figures 3(b)–(d). A comparison of the spectra in figures 3(a)–(d) reveals minor variations in intensity, but no qualitative changes in the spectral shape. The latter implies that the exchange-split transitions and hence the point-group symmetry (Γ_4) of the magnetic Mn^{3+} order are unaffected by the chemical doping. This is further corroborated by figure 3(e) showing temperature-dependent SHG measurements on ErMnO$_3$ ($x = 0$) and Er$_{1-x}$Ca$_x$MnO$_3$ ($x = 0.01$), i.e., the lowest and highest doping levels we investigated. In both cases the magnetic SHG signal vanishes at $T_N \approx 80$ K. This leads us to the conclusion that the antiferromagnetic ordering and the specific triangular spin structure (Γ_4-symmetry) of the parent compound ErMnO$_3$ persist under moderate chemical doping.

In order to test if this robustness of the antiferromagnetic order extends to the antiferromagnetic domain distribution, we further recorded spatially resolved SHG images at 20 K at a photon energy of 2.44 eV. This leads to the antiferromagnetic domains shown in figure 4 for ErMnO$_3$, Er$_{1-x}$Zr$_x$MnO$_3$, and Er$_{1-x}$Ca$_x$MnO$_3$. Here, antiferromagnetic domain walls are visible as dark lines, because SHG light from opposite domains exhibits a relative 180° phase shift and thus interferes destructively at the walls [30]. Note that when we talk about antiferromagnetic domains, we are in fact referring to *free* antiferromagnetic domains. These antiferromagnetic domains are not coupled to the coexisting ferroelectric domains in figure 2 [5], permitting an independent response to the applied chemical doping. The observed large extension of the antiferromagnetic domains is consistent with previous publications on domains in RMnO$_3$ systems and rather typical for antiferromagnetic 180° domains [3, 4, 31]. The data presented in figure 4 indicate that the antiferromagnetic domain walls are meandering in the *ab*-plane in an isotropic way without showing any indication of a doping dependence. Thus, the spatially resolved data are in agreement with the spectroscopic SHG data and demonstrate that the

antiferromagnetic domain structure in $Er_{1-x}Ca_xMnO_3$ and $Er_{1-x}Zr_xMnO_3$, like the ferroelectric domain distribution, is unperturbed by the chemical doping.

3. Summary

In summary, we grew single-crystals of Ca^{2+}- and Zr^{4+}-doped $ErMnO_3$ and showed experimentally that the bulk conductance of the multiferroic p-type semiconductor $ErMnO_3$ can readily be enhanced or suppressed by hole or electron doping, respectively. Spatially resolved imaging of the ferroelectric and antiferromagnetic domain structures in undoped and doped systems revealed that the key characteristics of the domain patterns are robust against moderate chemical substitutions. The results are expected to be independent of $R = Er$ and hence applicable to the whole hexagonal $RMnO_3$ series. With our work we demonstrated that electronic properties of semiconducting geometric multiferroics can be modified by introducing impurities, analogous to conventional semiconductors, while sustaining their intrinsic electric and magnetic domain structures. This opportunity provides a promising pathway for optimizing and fine-tuning the functionality of ferroic domains and is also of importance for related fields such as domain-wall engineering. Here, chemical doping may be used to ultimately tune the functional physical domain-wall properties of hexagonal manganites [10, 32] towards a technologically feasible working range [33].

Acknowledgments

References

[1] Fiebig M 2005 *J. Phys. D: Appl. Phys.* **38** 123
[2] Cheong S-W and Mostovoy M 2007 *Nat. Mater.* **6** 13
[3] Matsubara M, Manz S, Mochizuki M, Kubacka T, Iyama A, Aliouane N, Kimura T, Johnson S, Meier D and Fiebig M 2015 *Science* **348** 1112
[4] Meier M, Maringer M, Lottermoser T, Becker P, Bohatý L and Fiebig M 2009 *Phys. Rev. Lett.* **102** 107202
[5] Fiebig M, Lottermoser T, Fröhlich D, Goltsev A V and Pisarev R V 2002 *Nature* **419** 818
[6] Choi T, Horibe Y, Yi H T, Choi Y J, Wu W and Cheong S-W 2010 *Nat. Mater.* **9** 253
[7] Van Aken B B, Palstra T T M, Filippetti A and Spaldin N A 2004 *Nat. Mater.* **3** 164
[8] Griffin S M, Lilienblum M, Delaney K T, Kumagai Y, Fiebig M and Spaldin N A 2012 *Phys. Rev.* X **2** 041022
[9] Chae S C, Lee N, Horibe Y, Tanimura M, Mori S, Gao B, Carr S and Cheong S-W 2012 *Phys. Rev. Lett.* **108** 167603
[10] Meier D, Seidel S, Cano A, Delaney K, Kumagai Y, Mostovoy M, Spaldin N A, Ramesh R and Fiebig M 2012 *Nat. Mater.* **11** 284
[11] Geng Y, Das H, Wysocki A L, Wang X, Cheong S-W, Mostovoy M, Fennie C J and Wu W 2014 *Nat. Mater.* **13** 163
[12] Geng Y, Lee N, Choi Y J, Cheong S-W and Wu W 2012 *Nano Lett.* **12** 6055
[13] Salje E K H 2010 *Chem. Phys. Chem.* **11** 940
[14] Fiebig M, Fröhlich D and Leute S 1998 *J. Appl. Phys.* **83** 6560
[15] Kroemer H 2001 *Mod. Rev. Phys.* **73** 783
[16] Liu P, Cheng Z X, Du Y and Wang X L 2010 *J. Phys. D: Appl. Phys.* **43** 325002
[17] Asokan K *et al* 2009 *Appl. Phys. Lett.* **95** 131901
[18] Van Aken B B, Bos J-W G, de Groot R A and Palstra T T M 2001 *Phys. Rev.* B **63** 125127
[19] Fiebig M, Pavlov V V and Pisarev R V 2005 *J. Opt. Soc. Am.* B **22** 96
[20] Jungk T, Hoffmann Á, Fiebig M and Soergel E 2010 *Appl. Phys. Lett.* **97** 102902
[21] Lorenz B 2013 *ISRN Condens. Matter Phys.* **2013** 497073
[22] Meier D, Ryll H, Kiefer K, Hoffmann J U, Ramesh R and Fiebig M 2012 *Phys. Rev.* B **86** 184415
[23] Rao G V S, Wanklyn B M and Rao C N R 1971 *J. Phys. Chem. Solids* **32** 345
[24] Yan Z, Meier D, Schaab J, Ramesh R, Samoulon E and Bourret E 2015 *J. Cryst. Growth* **409** 75
[25] Katsufuji T, Mori S, Masaki M, Moritomo Y, Yamamoto N and Takagi H 2001 *Phys. Rev.* B **64** 104419
[26] Ren P, Fan H and Wang X 2013 *Appl. Phys. Lett.* **103** 152905
[27] Remsen S and Dabrowski B 2011 *Chem. Mater.* **23** 3818
[28] Fiebig M, Fröhlich D, Kohn K, Leute S, Lottermoser T, Pavlov V V and Pisarev R V 2000 *Phys. Rev. Lett.* **84** 5620
[29] Iizuka-Sano T, Hanamura E and Tanabe Y 2001 *J. Phys.: Condens. Matter* **13** 3031
[30] Petukhov A V, Lyubchanskii I L and Rasing T 1997 *Phys. Rev.* B **56** 2680
[31] Zimmermann A S, Meier D and Fiebig M 2014 *Nat. Commun.* **5** 4796
[32] Wu W, Horibe Y, Lee N, Cheong S-W and Guest J R 2012 *Phys. Rev. Lett.* **108** 077203
[33] Schaab J, Cano A, Lilienblum M, Yan Z, Bourret E, Ramesh R, Fiebig M and Meier D 2016 *Adv. Electron. Mater.* **2** 1500195